Accepted Manuscript

Title: Enzyme- and metal-free electrochemical sensor for highly sensitive superoxide anion detection based on nitrogen doped hollow mesoporous carbon spheres

Author: <ce:author id="aut0005" author-id="S0013468616327554-cad71b8ef83b08e5e19f7dbd6aae09a9"> Li Liu<ce:author id="aut0010" author-id="S0013468616327554-e6ef8597e7feeff024fa1c5d33b5c5d1"> Hongli Zhao<ce:author id="aut0015" author-id="S0013468616327554-aa02fe0f5b0f93f625ed5c0fb383b963"> Libo Shi<ce:author id="aut0020" author-id="S0013468616327554-5f95a1bdde2e92e4d5d460fb8177e964"> Minbo Lan<ce:author id="aut0025" author-id="S0013468616327554-041494deae30fc2db6b4ff8c6e77da97"> Hongwei Zhang<ce:author id="aut0030" author-id="S0013468616327554-d13696a68f9a252c3fc89dc0dff11ba2"> Chengzhong Yu

Please cite this article as: Li Liu, Hongli Zhao, Libo Shi, Minbo Lan, Hongwei Zhang, Chengzhong Yu, Enzyme- and metal-free electrochemical sensor for highly sensitive superoxide anion detection based on nitrogen doped hollow mesoporous carbon spheres, Electrochimica Acta http://dx.doi.org/10.1016/j.electacta.2016.12.182
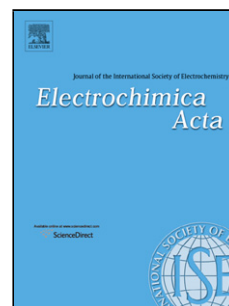
# Enzyme- and metal-free electrochemical sensor for highly sensitive superoxide anion detection based on nitrogen doped hollow mesoporous carbon spheres

Li Liu [a], Hongli Zhao [a,*], Libo Shi [a], Minbo Lan [a,b,*], Hongwei Zhang [c], Chengzhong Yu [c]

[a] Shanghai Key Laboratory of Functional Materials Chemistry, School of Chemistry and Molecular Engineering, East China University of Science and Technology, Shanghai 200237, PR China

[b] State Key Laboratory of Bioreactor Engineering, East China University of Science and Technology, Shanghai 200237, PR China

[c] Australian Institute for Bioengineering and Nanotechnology, The University of Queensland, Brisbane, Queensland 4072, Australia

* Corresponding authors. E-mails: honglizhao@ecust.edu.cn; (H. Zhao); minbolan@ecust.edu.cn; (M. Lan)

## Graphical abstract

A highly sensitive enzyme- and metal-free electrochemical sensor for superoxide anion ($O_2^{\bullet -}$) detection has been developed based on nitrogen doped hollow mesoporous carbon spheres (N-HMCS) modified screen-printed carbon electrodes (N-HMCS/SPCE).
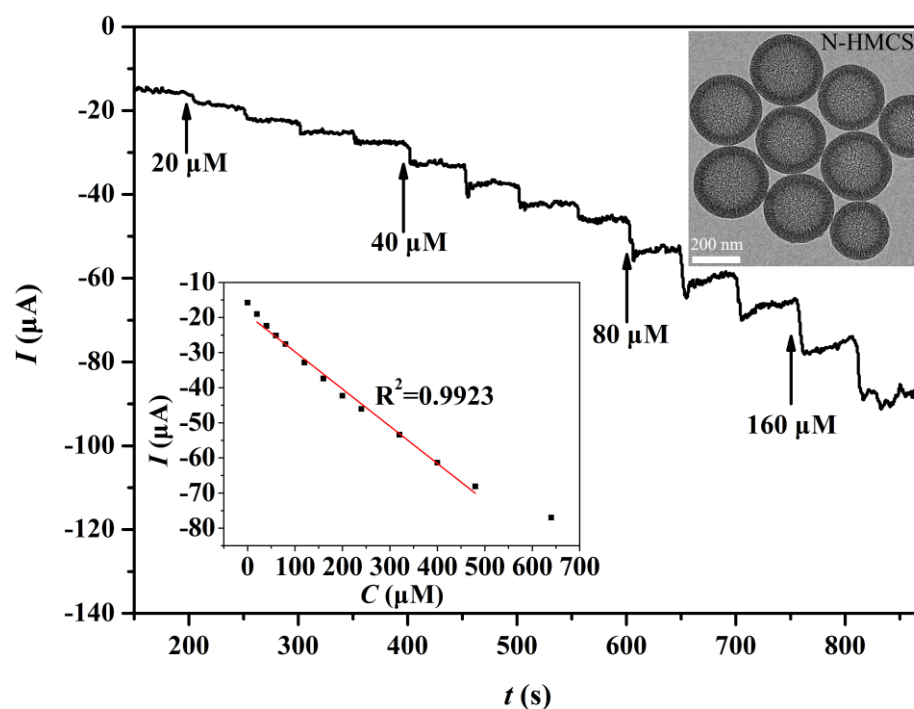
**Abstract:** In this work, a highly sensitive enzyme- and metal-free electrochemical method for superoxide anion ($O_2^{\bullet -}$) detection has been developed by employing screen-printed carbon electrodes (SPCE) modified by nitrogen doped hollow mesoporous carbon spheres (N-HMCS). For comparison, solid carbon spheres (SCS) and hollow mesoporous carbon spheres (HMCS) were also synthesized to fabricate the modified SPCE. Compared with SCS/SPCE and HMCS/SPCE, N-HMCS/SPCE displayed a higher electrochemical performance. When applied for electrochemical detection of

$O_2^{\bullet-}$, N-HMCS/SPCE exhibited a high sensitivity of 1.49 µA cm$^{-2}$ µM$^{-1}$, better than SCS/SPCE and HMCS/SPCE and many of enzyme- or metal-based superoxide anion sensors. N-HMCS is expected to become a new generation of sensing materials for electrochemical analysis of $O_2^{\bullet-}$.

**Keywords:** Nitrogen doped hollow mesoporous carbon spheres; electrochemical sensor; superoxide anion; highly sensitive

## 1. Introduction

Superoxide anion ($O_2^{\bullet-}$), as one kind of important reactive oxygen species (ROS), has a close relationship with some diseases such as neurodegeneration, atherosclerosis, diabetes and cancer [1-3]. For the detection of $O_2^{\bullet-}$, the enzyme-based electrochemical sensors have been developed as a favorable strategy. Among them, Cu, Zn-superoxide dismutase (Cu, Zn-SOD) [4-6] and cytochrome c [7-9] as the main enzymes were employed to fabricate $O_2^{\bullet-}$ enzymatic sensors. However, enzyme is vulnerable to the external conditions, such as pH, temperature and humidity, which have negative impact on the stability and reusability of enzyme-based sensors. In order to avoid these weaknesses, developing enzyme-free sensors for determination of $O_2^{\bullet-}$ is an attractive approach. At present, a few enzyme-free superoxide sensors have been reported based on narigin-copper complex [10], Pt nanoparticles covalently bonded to multi-walled carbon nanotubes [11] and copper-zinc alloy nanoparticles [12]. These good results

encouraged us to explore alternative non-toxic and low-cost materials as enzyme-free sensors for determination of $O_2^{\bullet-}$.

Recently, hollow mesoporous carbon spheres (HMCS) with superior structure features have gained extensive attention with widespread applications in the fields of catalysis [13, 14], adsorption [15-18], drug delivery [19], and energy storage [20, 21] due to their chemical inertness, high specific surface area, good electrical conductivity and biocompatibility. Moreover, the presence of mesoporous channels on the carbon shells of HMCS is beneficial for the mass transport and/or charge transfer between sensors and analytes [22]. Mesoporous carbon materials also have a high density of edge-plane-like defective sites which can promote the electron transfer to analytes and thereby enhance electrochemical activity at the electrodes [23, 24]. Nevertheless, using HMCS for electrochemical applications has received little attention [25]. In addition, it is well known that incorporation of heteroatoms, such as N, B, P, and S atoms [26-29], into the carbon matrix can largely improve their physicochemical properties [30]. Among these, N-doped is a promising strategy because the strong electron donor nature of N can supply negative charges to delocalized $\pi$ bond of $sp^2$ hybridized carbon skeleton so as to enhance electron transport properties and chemical reactivity [31-33]. Until now, a variety of N-containing carbons including graphene-based materials [34], carbon nanotubes [35], microporous or mesoporous carbons [36, 37] and carbon nanofibers [38] have been successfully utilized in many fields. N-doped hollow mesoporous carbon spheres (N-HMCS) also have been synthesized by various methods [39-41], but they were mainly employed as an efficient catalysis for oxygen reduction

reaction [42-44], and their applications in the field of electrochemical sensors for $O_2^{\bullet-}$ detection have been scarcely reported.

In this work, we focused on employing N-HMCS as an efficient enzyme-free sensing material for directly electrochemical detection of superoxide anion. The solid carbon spheres (SCS) and HMCS were applied to investigate the impact on the determination of $O_2^{\bullet-}$ from the different morphology. Based on the unique features of HMCS, such as good conductivity, large pore size/volume and high specific surface area, HMCS/SPCE exhibited much better detection performance for $O_2^{\bullet-}$ than SCS/SPCE. Further, owing to nitrogen doping, N-HMCS/SPCE showed extremely high sensitivity for quantification of $O_2^{\bullet-}$ even superior to many of metal-based or enzyme-based sensors.

## 2. Experimental

2.1. Reagents and apparatus

Tetrapropyl orthosilicate (TPOS), potassium superoxide, eighteen-crown-6 and anhydrous dimethyl sulfoxide (DMSO) were purchased from Aladdin Industrial Inc.. Ascorbic acid (AA), dopamine (DA), glucose (Glu), uric acid (UA), 4-acetaminophen (AP) and glutathione (GSH) were obtained from Sigma-Aldrich. All other chemicals were in analytical grade and used without further purification.

Nitrogen adsorption-desorption isotherms were measured on an ASAP 2020 (Micromeritics). A scanning electron microscope (SEM, JSM-6360LV, JEOL) was utilized to observe the surface morphology of carbon spheres. The transmission electron microscope (TEM, JEM-1400, JEOL) was used to capture the morphology of carbon spheres. The surface composition of carbon spheres was recorded by X-ray

photoelectron spectrometer (XPS, ESCALAB250Xi, Thermo Fisher). Raman spectra were obtained with an InVia Reflex Raman microscope. All electrochemical experiments were performed at room temperature on a CHI660D workstation equipped with a conventional three-electrode system consisting of a screen-printed working electrode, a platinum wire counter electrode, and an Ag/AgCl reference electrode.

2.2 Preparation of HMCS, N-HMCS and SCS

The HMCS was synthesized according to a report [45]. Typically, TPOS (3.46 mL, 12 mmol) was mixed with solution containing ethanol (70 mL), $H_2O$ (10 mL) and aqueous ammonia (3 mL) under constant stirring for 15 minutes. Then, formaldehyde (0.56 mL) and resorcinol (0.4 g) were added and the system was kept stirring for 24 h at room temperature. The products were collected by centrifugation, washed with deionized water and ethanol for several times, and dried at 50 $^o$C in the vacuum oven. HMCS were finally obtained after carbonization at 700 $^o$C (5 $^o$C min$^{-1}$) for 5 h under the $N_2$ atmosphere, followed by an etching process with 2 M NaOH at 80 $^o$C to remove silica. Further, a half of prepared HMCS was dispersed in aqueous ammonia (50 mL) and then the mixture was reacted for 9 h at 180 $^o$C in the 100 mL Teflon-lined autoclave to gain the N-HMCS.

The synthesis of SCS was a similar process as followed: resorcinol (0.24 g) and formaldehyde (0.36 mL) reacted with the mixture containing ethanol (70 mL), ultra-pure water (10 mL) and aqueous ammonia (3 mL) for 12 h in ambient temperature with constant stirring. After the above mixed solution was centrifuged and washed by water

and ethanol for several times then dried it, the obtained solid product was carbonized at 700 $^{\circ}$C (5 $^{\circ}$C min$^{-1}$) under N$_2$ for 5 h.

2.3 Fabrication of the modified electrodes

The home-made screen-printed carbon electrodes (SPCE) with a working area of 0.071 cm$^2$ were served as the substrate according to our previous work [46]. 5 mg N-HMCS was added into 5 mL ultrapure water and sonicated to form a well-dispersed mixture. Then, 10 μL of the mixture and 2 μL of 0.05 wt% Nafion were drop-casted onto SPCE successively, and the N-HMCS modified electrodes (N-HMCS/SPCE) were finally formed after dried. The HMCS modified electrodes (HMCS/SPCE) and SCS modified electrodes (SCS/SPCE) were fabricated with a similar method, and the bare SPCE was only treated with 2 μL of 0.05 wt% Nafion.

2.4 Generation of superoxide anion

The superoxide anion was generated from the KO$_2$-DMSO system according to our previous work [47]. Briefly, a stock solution of KO$_2$ was prepared by adding KO$_2$ into anhydrous DMSO, containing 18-crown-6 that can increase the solubility of KO$_2$. After sonicating the solution for 2 min, KO$_2$ was dissociated and produced O$_2$$^{\bullet-}$. The concentration of O$_2$$^{\bullet-}$ was determined to be 8 μM μL$^{-1}$ by UV-Vis spectroscope with the molar absorptivity of O$_2$$^{\bullet-}$ in DMSO (2006 M$^{-1}$ cm$^{-1}$ at 271 nm) [48].

2.5 Electrochemical measurement

The electrochemical behaviors of modified electrodes were investigated using cyclic voltammetric (CV), chronoamperometric, chronocoulometric, and electrochemical impedance spectroscopy (EIS) techniques, respectively. CV measurements were

performed in stationary electrolyte solution. The chronoamperometric experiments were implemented by successively adding the analytes into 5 mL 0.1 M phosphate buffer solution (PBS, pH 7.4) under constantly stirring. Chronocoulometric measurements were carried out in the 0.1 mM $K_3[Fe(CN)_6]$ containing 1 M KCl. And EIS was gained in the 5 mM $K_3[Fe(CN)_6]$ (0.1 M KCl) solution and the equivalent circuit of Nyquist plots was simulated using the ZSimpWin software.

For real samples analysis, the recovery of the sensor was assessed using a calibration curve method in the Dulbecco's modified Eagle's medium (DMEM) containing 10% fetal bovine serum (FBS) and 1% penicillin/streptomycin. The real time monitoring of $O_2^{•-}$ by N-HMCS/SPCE in living cells was also evaluated. The proposed electrodes were tried to capture $O_2^{•-}$ released from living cells L929 suspension stimulated by 30 μL Zymosan solution (5 mg/mL) at -0.15 V.

## 3. Results and discussion

3.1 Characterization of carbon spheres

The morphology of SCS, HMCS and N-HMCS was characterized by SEM and TEM. Three prepared carbon materials all exhibited a uniform spherical morphology with a mean size of 270 nm (**Fig. 1A, C** and **D**). Compared to SCS with a solid structure (the inset of **Fig. 1A**), a characteristic hollow structure was observed for HMCS (inset of **Fig. 1C**) with an interior hollow cavity and a porous shell. The morphology of HMCS was not changed after hydrothermal treatment at 180 °C by comparing **Fig. 1C** and **Fig. 1B**.

The textural properties of SCS, HMCS, and N-HMCS were measured by nitrogen adsorption/desorption isotherms. The typical isotherm of SCS (**Fig. 1D**) belongs to type

I curve, suggesting the existence of microporous; while both HMCS and N-HMCS (**Fig. 1E** and **F**) exhibit the type IV isotherm which is the characteristic feature of mesoporous material. As shown in the pore size distribution curves calculated by Barrett-Joyner-Halenda (BJH) method (the inset of **Fig. 1D, E** and **F**), the average pore size is approximately 1.9 nm for SCS which may be caused during the process of carbonation, while 7.5 nm for HMCS and 7.4 nm for N-HMCS. The Brunauer–Emmett–Teller (BET) surface area of SCS, HMCS and N-HMCS were calculated to be 584.5, 1189.4 and 1181.7 $m^2/g$ and the pore volume were measured to be 0.05, 2.05 and 2.06 $cm^3/g$, respectively.

<center>(*Please insert Figure 1 here*)</center>

The surface chemical composition of the three carbon spheres was determined by XPS. As shown in the XPS survey spectra (**Fig. S1**), the SCS and HMCS samples possessed only two typical peaks for C1s and O1s, while the N-HMCS exhibited an addition peak for N1s with a content of 4.4%. The whole nitrogen content of N-HMCS was also measured by elementary analysis (6.3%), slightly higher than that measured from XPS. The N1s spectrum can be separated into four signal peaks with the binding energies of 398.26 eV, 399.49 eV, 400.51 eV and 403.55 eV related to pyridinic N, amino or imino N, pyrrolic N, and quaternary N, respectively (**Fig. 2A**). The presence of pyridinic N (28.5%), pyrrolic N (26.7%), and quaternary N (16.9%) species suggests that nitrogen was mainly incorporated into the carbon structure, and because the post-processing method was adopted to introduce the nitrogen, there existed some amino or imino N (27.9%), in accordance with literature reports [49, 50].

The graphitic order of the three carbons was detected by Raman spectroscopy (**Fig. 2B**). The G band at ~1598 cm$^{-1}$ stands for an $E_{2g}$ mode of graphite related to the vibration of sp$^2$-hybridized carbon atoms of C-C. The peak at ~1354 cm$^{-1}$ (D band) is connected to the vibration of carbon atoms with dangling bands in the plane termination of disordered graphite [51]. In addition, the intensity ratio of D band and G band ($I_D/I_G$) reflects the order degree of carbon. The values of $I_D/I_G$ of SCS, HMCS and N-HMCS were calculated to be 1.13, 1.12 and 1.25, respectively, suggesting that the SCS and HMCS have similar defect degrees and the defect sites of carbon spheres were increased with the introduction of nitrogen [52, 53] which may provide many active sites for electron transfer.

(*Please insert Figure 2 here*)

The above characterizations demonstrate that the prepared HMCS and SCS possess similar particle size and surface composition. The structural difference between HMCS and SCS provides the opportunity to investigate the influence of hollow mesoporous structure on the electrochemical performance for $O_2^{\bullet-}$ detection. At the preparation process of N-HMCS, through the hydrothermal treatment with aqueous ammonia, structural features of HMCS still remained, while the defect sites on the surface have been increased as nitrogen incorporated, which will provide more electroactive sites for $O_2^{\bullet-}$, and may have an improvement in the sensitivity.

3.2 Electrochemical characterization

The electrochemical properties of the three carbon modified electrodes were investigated by CV and EIS. The typical CV of Fe(CN)$_6^{3-/4-}$ is a valid tool for evaluating

the kinetic barrier of the interface [54]. As shown in the **Fig. 3A**, the potential between the anodic and cathodic peaks ($\Delta E_p$) was 0.45 V for bare SPCE, 0.33 V for SCS/SPCE, 0.22 V for HMCS/SPCE and 0.20 V for N-HMCS/SPCE, respectively. It was also observed that the redox peak currents increased with the decrease of $\Delta E_p$. The smaller value of $\Delta E_p$ and the higher redox peak currents indicate the better electron transfer ability [25, 55]. The order in terms of electron transfer rate for various electrodes follows the following sequence: N-HMCS/SPCE > HMCS/SPCE > SCS/SPCE > bare SPCE.

EIS is an effective technique to determine the electron-transfer resistance at the electrode -electrolyte interface. From the Nyquist plot (**Fig. 3B**), the charge-transfer resistances ($R_{ct}$) of N-HMCS/SPCE, HMCS/SPCE, SCS/SPCE and bare SPCE are calculated to be 55.6 $\Omega$, 155.9 $\Omega$, 4579 $\Omega$ and 4671 $\Omega$, respectively, which is consistent with the above result of CV characterizations. The pretty low $R_{ct}$ of HMCS/SPCE can be attributed to the merits of the unique mesoporous and hollow structures of HMCS, compared with the $R_{ct}$ of SCS/SPCE. Moreover, with the help of strong electron donor nature of N atom, the N-HMCS/SPCE show lower $R_{ct}$ than that of HMCS/SPCE.

The electrochemically active surface area ($A$), which is closely related to the electrocatalytic ability of the sensors [56], can be assessed by using the chronocoulometric technique based on the following Anson equation [57]:

$$Q = Q_{dl} + Q_{ads} + 2nFAC(Dt/\pi)^{1/2},$$

where $Q_{dl}$ is the double layer charge; $Q_{ads}$ is the Faradaic charge; $n$ is the number of transferred electrons; $F$ is the Faraday constant; $C$ is the concentration of electrolytes; and $D$ is the diffusion coefficient, taking a value of $7.6 \times 10^{-6}$ cm$^2$/s (25 $^o$C) in 0.1 mM

K$_3$[Fe(CN)$_6$] containing 1 M KCl. The $Q$-$t$ and $Q$-$t^{1/2}$ pots of bare SPCE, SCS/SPCE, HMCS/SPCE and N-HMCS/SPCE are shown in **Fig 3C**. According to the $Q$-$t^{1/2}$ plots, $A$ is calculated to be 12.2726 cm$^2$ for HMCS/SPCE, which is much larger than that of SCS/SPCE (0.2593 cm$^2$) and bare SPCE (0.1732 cm$^2$). This distinctly high $A$ value of HMCS/SPCE is related to the large specific surface of hollow mesoporous structure. With the nitrogen doped, the surface active sites are further significantly increased, so that $A$ value of N-HMCS/SPCE is also improved to 15.9535 cm$^2$. This larger active surface of N-HMCS/SPCE may benefit to enhancing the sensitivity of sensors.

The electrochemistry behavior of N-HMCS/SPCE in 5 mM K$_3$[Fe(CN)$_6$] at different scan rates from 10 to 100 mV s$^{-1}$ was further investigated. As shown in **Fig. 3D**, $\Delta E_p$ increased along with the increase of scan rates and $\Delta I_p$ was found to be linearly proportional to $v^{1/2}$ (the inset of **Fig. 3D**), which suggests a diffusion-controlled process on the surface of N-HMCS/SPCE.

(*Please insert Figure 3 here*)

3.3 Electrochemical performance of SCS/SPCE, HMCS/SPCE and N-HMCS/SPCE towards superoxide anion detection

The electrochemical properties of modified electrodes towards the detection of O$_2$$^{\bullet-}$ were evaluated by the CV measurements. **Fig. 4A** and **Fig. 4B** display the CV curves of the HMCS/SPCE and N-HMCS/SPCE in 0.1 M deoxygenated PBS (pH 7.4) with the absence and presence of 400 μM O$_2$$^{\bullet-}$, respectively. When the potential was varied from -0.6 V to 0.6 V, the HMCS/SPCE showed a wide reduction peak from -0.10 V to -0.45 V, while a significant sharp reduction peak occurred from 0 V to -0.2 V for N-

HMCS/SPCE with higher current density. This phenomenon indicates that N-HMCS/SPCE exhibits better ability to promote the reduction process of $O_2^{\bullet-}$ than that of HMCS/SPCE.

The reduction peak of the above CV curves after adding of $O_2^{\bullet-}$ should be produced from the electrochemical reduction of $O_2^{\bullet-}$ on the modified electrodes surface, illustrated as the equation: $O_2^{\bullet-} + 2\ H^+ + e^- = H_2O_2$. This mechanism can be explained from the following aspects: firstly, we eliminated the possibility that the reduction signal originated from the electrochemical reduction of $H_2O_2$ by comparing the current responses on N-HMCS/SPCE with adding 80 μM $O_2^{\bullet-}$ and 40 μM $H_2O_2$ at -0.15 V. The $O_2^{\bullet-}$ can undergo disproportionation into $H_2O_2$ and $O_2$ in the aqueous solution [11]. According to the disproportionation reaction equation ($2H^+ + 2O_2^{\bullet-} = H_2O_2 + O_2$), if the reduction signal was produced by the $H_2O_2$ generated from the $O_2^{\bullet-}$, the current response intensity of 80 μM $O_2^{\bullet-}$ and 40 μM $H_2O_2$ would be equal. Actually, it is obvious that the current response of $H_2O_2$ is much smaller than that of $O_2^{\bullet-}$ (shown in **Fig. S2**). Then, we conducted another experiment and the result is shown in **Fig. S3**. When $O_2^{\bullet-}$ was added, current response can be observed increased. And further injection of superoxide dismutase (SOD) resulted in the current responses back to the base level. This decay of current response is caused by the fact that the high catalytic activity of specific enzyme SOD accelerates the scavenger of $O_2^{\bullet-}$ [58]. In addition, several works have demonstrated that some carbonaceous materials including hydrophilic carbon clusters (HCCs) [59, 60], fullerene ($C_{60}$) [61] and fullerene derivatives [62] show SOD mimetic properties, which ensure that $O_2^{\bullet-}$ can be efficiently reduced on the surface of

mesoporous carbon modified electrodes at reduction potential. From the above, we can draw the conclusion that the origin of reduction signal is from the dismutation of $O_2^{\bullet-}$ on the electrode surface.

Before amperometric detecting of $O_2^{\bullet-}$, the detection potential and the presence of oxygen have been optimized. The amperometric responses of HMCS/SPCE in the deoxygenated solution and air saturated solution were recorded as shown in **Fig. S4**. The signal intensity of the latter is only two-thirds of the former. This is related to the disproportionation of $O_2^{\bullet-}$ on the surface of carbon materials that can generate $O_2$, thus the dissolved $O_2$ in the PBS will suppress the disproportionation reaction, and then influence the process of electrochemical reduction of $O_2^{\bullet-}$. Therefore, the detection conditions should be deoxygenated. As the **Fig. S5** shown, the optimum potential for $O_2^{\bullet-}$ detection was at -0.25 V for HMCS/SPCE (also for SCS/SPCE) and -0.15 V for N-HMCS/SPCE. It indicates that $O_2^{\bullet-}$ reduction on the N-HMCS/SPCE occurs with a small overpotential than that on the HMCS/SPCE.

A comparison of the current responses on different carbon spheres modified electrodes upon successive additions of 40 μM $O_2^{\bullet-}$ was obtained as depicted in **Fig. 4C.** HMCS/SPCE and N-HMCS/SPCE display obvious stepwise increases of the current responses upon addition of the analyte, but the response of SCS/SPCE is so small that can be neglected. N-HMCS/SPCE shows the best sensitivity for $O_2^{\bullet-}$ detection, which is 99.84 and 1.29 fold higher than those of SCS/SPCE and HMCS/SPCE, respectively. The results are mainly attributed to the following reasons: (1) the large surface area and mesoporous hollow structure of N-HMCS provides abundant electrochemical active

sites. (2) The high electrical conductivity of N-HMCS leads to fast electron transfer during the process of electrochemical reduction of $O_2^{\bullet-}$.

(*Please insert Figure 4 here*)

The typical whole chronoamperometric responses of the N-HMCS/SPCE for $O_2^{\bullet-}$ at -0.15 V were recorded. As depicted in **Fig. 4D,** the changes in the current on the addition of $O_2^{\bullet-}$ until 480 μM is proportional to the concentration of $O_2^{\bullet-}$, and the sensitivity is calculated to be 1493.2 μA $cm^{-2}$ $mM^{-1}$ based on the working area 0.071 $cm^2$ of the electrodes. Beyond this concentration, the slope is decreased, suggesting the saturation limit the N-doped active surface. The limit of detection (LOD) is further calculated to be 2.2 μM based on the signal-to-noise ratio of three protocol (S/N=3). In addition, the analytical performance of N-HMCS/SPCE in this work is also compared with other $O_2^{\bullet-}$ sensors as listed in **Table 1**. It suggests that N-HMCS based sensors without any enzyme or metallic nanomaterials still show superior sensitivity to other sensors.

(*Please insert **Table 1** here*)

In addition, the selectivity, repeatability and stability of the N-HMCS/SPCE were estimated respectively. The experimental results indicate the substances, including glucose, glutathione (GSH), ascorbic acid (AA), uric acid (UA), acetaminophen (AP) and dopamine (DA) have little effect on the amperometric detection of $O_2^{\bullet-}$, demonstrating that the N-HMCS/SPCE have good selectivity towards $O_2^{\bullet-}$ (shown in **Fig. S6**). The N-HMCS/SPCE also shows an excellent repeatability with a RSD (relative standard deviation) of 1.5% (n=6) and a good long-term stability with the sensitivity remained 91.4% of its initial sensitivity after 25 days.

3.4 Real sample analysis

DMEM containing 10% FBS and 1% penicillin/streptomycin was used to mimic the environment of cell culture. Through a calibration curve method, the recovery in that solution was determined to be 92.37%, 93.13% and 90.63% with added 80, 160 and 240 $\mu$M $O_2^{\bullet-}$ (**Table S1**). The results indicate that the N-HMCS/SPCE can be applied to detect $O_2^{\bullet-}$ in a relatively complicated system. Furthermore, in order to investigate the possibility of N-HMCS/SPCE applied to real time monitoring of $O_2^{\bullet-}$ in living cells, the electrodes were tested to capture $O_2^{\bullet-}$ released from living cells L929 which is cultured by our own laboratory and dispersed in the PBS (0.1M, pH 7.4). When 30 $\mu$L zymosan solution (5 mg/mL) was added to the cell suspension, zymosan will stimulate the inflammatory response of cells, and release a large number of $O_2^{\bullet-}$ instantaneously. The result is shown as the **Fig. S7**, and it can be seen that the current responses of the N-HMCS/SPCE increased rapidly with zymosan added in the L929 cells suspension, suggesting the generation of $O_2^{\bullet-}$. Subsequently, the $O_2^{\bullet-}$ signal intensity reduced slowly, and ultimately returned to baseline position. For comparison, when the same concentration of zymosan was added into 0.1 M PBS, there was no significant current response signal produced, which can be illustrated that the N-HMCS/SPCE can successfully capture the electrical signals of $O_2^{\bullet-}$ generated by living cells. Though this method is only suitable for qualitative analysis in living cells, the above results can still reveal the promising potential of the N-HMCS based sensor in the detection of $O_2^{\bullet-}$ for real sample analysis.

**4. Conclusions**

In summary, we have successfully fabricated enzyme- and metal-free $O_2^{\bullet-}$ electrochemical sensors. Compared with SCS and HMCS, it is demonstrated that N-HMCS provide more abundant electrochemical active sites and a higher electrical conductivity, leading to faster electron transfer during the process of electrochemical reduction of $O_2^{\bullet-}$. Therefore, N-HMCS/SPCE exhibit an outstanding performance for $O_2^{\bullet-}$ detection with a sensitivity of 1.49 $\mu A\,cm^{-2}\,\mu M^{-1}$, which is higher than that of many of enzyme- and metal- based $O_2^{\bullet-}$ sensors. In addition, the N-HMCS/SPCE electrochemical sensor can be applied in the detection of $O_2^{\bullet-}$ released from living cells. It is expected that the N-HMCS can be developed into a promising sensing material for $O_2^{\bullet-}$ determination, potentially for on-line $O_2^{\bullet-}$ analysis in the future.

**References:**

[1] W. Wang, H. Fang, L. Groom, A. Cheng, W. Zhang, J. Liu, X. Wang, K. Li, P. Han, M. Zheng, Superoxide flashes in single mitochondria, Cell, 134 (2008) 279-290.

[2] C. Calhau, A. Santos, Oxidative stress in the metabolic syndrome, in: R. Soares, C. Costa (Eds.), Oxidative stress, inflammation and angiogenesis in the metabolic syndrome, Springer, Netherlands, 2009, pp. 33-63.

[3] J. A. Knight, Reactive oxygen species and the neurodegenerative disorders, Ann. Clin. Lab. Sci., 27 (1997) 11-25.

[4] X. Wang, M. Han, J. Bao, W. Tu, Z. Dai, A superoxide anion biosensor based on direct electron transfer of superoxide dismutase on sodium alginate sol-gel film and its application to monitoring of living cells, Anal. Chim. Acta., 717 (2012) 61-66.

[5] J. Tang, X. Zhu, X. Niu, T. Liu, H. Zhao, M. Lan, Anamperometric superoxide anion radical biosensor based on SOD/PtPd-PDARGO modified electrode, Talanta, 137 (2015) 18-24.

[6] Z. Deng, Q. Rui, X. Yin, H. Liu, Y. Tian, In vivo detection of superoxide anion in bean sprout based on ZnO nanodisks with facilitated activity for direct electron transfer of superoxide dismutase, Anal. Chem., 80 (2008) 5839-5846.

[7] S. Gáspár, J. L. Marty, E. Gheorghiu, Cytochrome c-based amperometric sensors for superoxide detection: Where their signal comes from? Electroanalysis, 25 (2013) 448-452.

[8] X. J. Chen, A. C. West, D. M. Cropek, S. Banta, Detection of the superoxide radical anion using various alkanethiol monolayers and immobilized cytochrome c, Anal. Chem., 80 (2008) 9622-9629.

[9] M. K. Beissenhirtz, F. W. Scheller, F. Lisdat, A superoxide sensor based on a multilayer cytochrome c electrode, Anal. Chem., 76 (2004) 4665-4671.

[10] S. Madhurantakam, S. Selvaraj, N. Nesakumar, S. Sethuraman, J. B. B. Rayappan, U. M. Krishnan, Electrochemical enzymeless detection of superoxide employing naringin-copper decorated electrodes, Biosens. Bioelectron., 59 (2014) 134-139.

[11] S. K. Kim, D. Kim, J. M. You, H. S. Han, S. Jeon, Non-enzymatic superoxide anion radical sensor based on Pt nanoparticles covalently bonded to thiolated MWCNTs, Electrochim. Acta, 81 (2012) 31-36.

[12] B. Derkus, E. Emregul, K.C. Emregul, Copper-zinc alloy nanoparticle based enzyme-free superoxide radical sensing on a screen-printed electrode, Talanta, 134 (2015) 206-214.

[13] J. Wu, C. Jin, Z. Yang, J. Tian, R. Yang, Synthesis of phosphorus-doped carbon hollow spheres as efficient metal-free electrocatalysts for oxygen reduction, Carbon, 82 (2015) 562-571.

[14] Z. Yan, H. Meng, P.K. Shen, Y. Meng, H. Ji, Effect of the templates on the synthesis of hollow carbon materials as electrocatalyst supports for direct alcohol fuel cells, Int. J. Hydrog. Energy, 37 (2012) 4728-4736.

[15] L. Guo, X. Cui, Y. Li, Q. He, L. Zhang, W. Bu, J. Shi, Hollow mesoporous carbon spheres with magnetic cores and their performance as separable bilirubin adsorbents, Chem. Asian J., 4 (2009) 1480-1485.

[16] W. J. Liu, Y. X. Liu, X. Y. Yan, G. P. Yong, Y. P. Xu, S. M. Liu, One-pot synthesis of yolk-shell mesoporous carbon spheres with high magnetisation, J. Mater. Chem. A, 2 (2014) 9600-9606.

[17] L. Guo, L. Zhang, J. Zhang, J. Zhou, Q. He, S. Zeng, X. Cui, J. Shi, Hollow mesoporous carbon spheres-an excellent bilirubin adsorbent, Chem. Commun., 40 (2009) 6071-6073.

[18] W. Konicki, K. Cendrowski, X. Chen, E. Mijowska, Application of hollow mesoporous carbon nanospheres as an high effective adsorbent for the fast removal of acid dyes from aqueous solutions, Chem. Eng. J., 228 (2013) 824-833.

[19] W. Liu, F. Zhu, Y. Liu, Y. Xu, S. Liu, One-pot synthesis of hollow mesoporous carbon materials and their drug release properties, J. Mater. Sci., 50 (2015) 717-724.

[20] K. Zhang, Q. Zhao, Z. Tao, J. Chen, Composite of sulfur impregnated in porous hollow carbon spheres as the cathode of Li-S batteries with high performance, Nano Res., 6 (2013) 38-46.

[21] Y. Dai, H. Jiang, Y. Hu, Y. Fu, C. Li, Controlled synthesis of ultrathin hollow mesoporous carbon nanospheres for supercapacitor applications, Ind. Eng. Chem. Res., 53 (2014) 3125-3130.

[22] A. Walcarius, Mesoporous materials-based electrochemical sensors, Electroanalysis, 27 (2015) 1303-1340.

[23] M. Zhou, S. Guo, Electrocatalytic interface based on novel carbon nanomaterials for advanced electrochemical sensors, ChemCatChem, 7 (2015) 2744-2764.

[24] M. Zhou, L. Shang, B. Li, L. Huang, S. Dong, Highly ordered mesoporous carbons as electrode material for the construction of electrochemical dehydrogenase-and oxidase-based biosensors, Biosens. Bioelectron., 24 (2008) 442-447.

[25] C. Xiao, X. Chu, Y. Yang, X. Li, X. Zhang, J. Chen, Hollow nitrogen-doped carbon microspheres pyrolyzed from self-polymerized dopamine and its application in simultaneous electrochemical determination of uric acid, ascorbic acid and dopamine, Biosens. Bioelectron., 26 (2011) 2934-2939.

[26] C. Zhang, N. Mahmood, H. Yin, F. Liu, Y. Hou, Synthesis of phosphorus- doped graphene and its multifunctional applications for oxygen reduction reaction and lithium ion batteries, Adv. Mater., 25 (2013) 4932-4937.

[27] S. A. Wohlgemuth, R. J. White, M. G. Willinger, M. M. Titirici, M. Antonietti, A one-pot hydrothermal synthesis of sulfur and nitrogen doped carbon aerogels with enhanced electrocatalytic activity in the oxygen reduction reaction, Green Chem., 14 (2012) 1515-1523.

[28] D. Song, S. An, B. Lu, Y. Guo, J. Leng, Arylsulfonic acid functionalized hollow mesoporous carbon spheres for efficient conversion of levulinic acid or furfuryl alcohol to ethyl levulinate, Appl. Catal. B-Environ., 179 (2015) 445-457.

[29] L. Yang, S. Jiang, Y. Zhao, L. Zhu, S. Chen, X. Wang, Q. Wu, J. Ma, Y. Ma, Z. Hu, Boron-doped carbon nanotubes as metal-free electrocatalysts for the oxygen reduction reaction, Angew. Chem., 123 (2011) 7270-7273.

[30] Z. Yang, H. Nie, X. A. Chen, X. Chen, S. Huang, Recent progress in doped carbon nanomaterials as effective cathode catalysts for fuel cell oxygen reduction reaction, J. Power Sources, 236 (2013) 238-249.

[31] W. Wong, W. R. W. Daud, A. B. Mohamad, A. A. H. Kadhum, K. S. Loh, E. Majlan, Recent progress in nitrogen-doped carbon and its composites as electrocatalysts for fuel cell applications, Int. J. Hydro. Energy, 38 (2013) 9370-9386.

[32] Y. Zhang, X. Bo, A. Nsabimana, C. Luhana, G. Wang, H. Wang, M. Li, L. Guo, Fabrication of 2D ordered mesoporous carbon nitride and its use as electrochemical sensing platform for $H_2O_2$, nitrobenzene, and NADH detection, Biosens. Bioelectron., 53 (2014) 250-256.

[33] Y. Tang, B. L. Allen, D. R. Kauffman, A. Star, Electrocatalytic activity of nitrogen-doped carbon nanotube cups, J. Am. Chem. Soc., 131 (2009) 13200-13201.

[34] Y. Wang, Y. Shao, D.W. Matson, J. Li, Y. Lin, Nitrogen-doped graphene and its application in electrochemical biosensing, ACS Nano, 4 (2010) 1790-1798.

[35] M. Arjmand, K. Chizari, B. Krause, P. Pötschke, U. Sundararaj, Effect of synthesis catalyst on structure of nitrogen-doped carbon nanotubes and electrical conductivity and electromagnetic interference shielding of their polymeric nanocomposites, Carbon, 98 (2016) 358-372.

[36] T. Lin, I. W. Chen, F. Liu, C. Yang, H. Bi, F. Xu, F. Huang, Nitrogen-doped mesoporous carbon of extraordinary capacitance for electrochemical energy storage, Science, 350 (2015) 1508-1513.

[37] G. Ferrero, A. Fuertes, M. Sevilla, N-doped microporous carbon microspheres for high volumetric performance supercapacitors, Electrochim. Acta, 168 (2015) 320-329.

[38] J. Zhu, C. Chen, Y. Lu, Y. Ge, H. Jiang, K. Fu, X. Zhang, Nitrogen-doped carbon nanofibers derived from polyacrylonitrile for use as anode material in sodium-ion batteries, Carbon, 94 (2015) 189-195.

[39] J. Tang, J. Liu, C. Li, Y. Li, M.O. Tade, S. Dai, Y. Yamauchi, Synthesis of nitrogen-doped mesoporous carbon spheres with extra-large pores through assembly of diblock copolymer micelles, Angew. Chem. Int. Edit., 54 (2015) 588-593.

[40] C. Han, S. Wang, J. Wang, M. Li, J. Deng, H. Li, Y. Wang, Controlled synthesis of sustainable N-doped hollow core-mesoporous shell carbonaceous nanospheres from biomass, Nano Res., 7 (2014) 1809-1819.

[41] A.F. Arif, Y. Kobayashi, R. Balgis, T. Ogi, H. Iwasaki, K. Okuyama, Rapid microwave-assisted synthesis of nitrogen-functionalized hollow carbon spheres with high monodispersity, Carbon, 107 (2016) 11-19.

[42] T. Yang, J. Liu, R. Zhou, Z. Chen, H. Xu, S. Z. Qiao, M. J. Monteiro, N-doped mesoporous carbon spheres as the oxygen reduction reaction catalysts, J. Mater. Chem. A, 2 (2014) 18139-18146.

[43] J. Yan, H. Meng, F. Xie, X. Yuan, W. Yu, W. Lin, W. Ouyang, D. Yuan, Metal free nitrogen doped hollow mesoporous graphene-analogous spheres as effective electrocatalyst for oxygen reduction reaction, J. Power Sources, 245 (2014) 772-778.

[44] C. H. Hsu, J. Y. Jan, H. P. Lin, P. L. Kuo, Nitrogen-doped mesoporous carbon hollow spheres as a novel carbon support for oxygen reduction reaction, New J. Chem., 38 (2014) 5521-5526.

[45] H. Zhang, O. Noonan, X. Huang, Y. Yang, C. Xu, L. Zhou, C. Yu, Surfactant-free assembly of mesoporous carbon hollow spheres with large tunable pore sizes, ACS Nano, 10 (2016) 4579-4586.

[46] X. Niu, H. Zhao, M. Lan, Disposable screen-printed antimony film electrode modified with carbon nanotubes/ionic liquid for electrochemical stripping measurement, Electrochim. Acta, 56 (2011) 9921-9925.

[47] X. Zhu, X. Niu, H. Zhao, J. Tang, M. Lan, Immobilization of superoxide dismutase on Pt-Pd/MWCNTs hybrid modified electrode surface for superoxide anion detection, Biosens. Bioelectron., 67 (2015) 79-85.

[48] K. Thandavan, S. Gandhi, S. Sethuraman, J. B. B. Rayappanb, U. M. Krishnan. A novel nano-interfaced superoxide biosensor, Sens. Actuators B: Chem., 2013, 176: 884-892.

[49] G. Wang, L. T. Jia, Y. Zhu, B. Hou, D. B. Li, Y. H. Sun, Novel preparation of nitrogen-doped graphene in various forms with aqueous ammonia under mild conditions, RSC Adv., 2 (2012) 11249-11252.

[50] X. Wang, J. S. Lee, Q. Zhu, J. Liu, Y. Wang, S. Dai, Ammonia-treated ordered mesoporous carbons as catalytic materials for oxygen reduction reaction, Chem. Mater., 22 (2010) 2178-2180.

[51] A. C. Ferrari, D. M. Basko, Raman spectroscopy as a versatile tool for studying the properties of graphene, Nat. Nanotechnol., 8 (2013) 235-246.

[52] J. Y. Hwang, C. C. Kuo, L. C. Chen, K. H. Chen, Correlating defect density with carrier mobility in large-scaled graphene films: Raman spectral signatures for the estimation of defect density, Nanotechnology, 21 (2010) 465705.

[53] Y. Cao, H. Yu, J. Tan, F. Peng, H. Wang, J. Li, W. Zheng, N. B. Wong, Nitrogen-, phosphorous- and boron-doped carbon nanotubes as catalysts for the aerobic oxidation of cyclohexane, Carbon, 57 (2013) 433-442.

[54] B. Rezaei, N. Majidi, H. Rahmani, T. Khayamian, Electrochemical impedimetric immunosensor for insulin like growth factor-1 using specific monoclonal antibody-nanogold modified electrode, Biosens. Bioelectron., 26 (2011) 2130-2134.

[55] R. S. Nicholson, Theory and application of cyclic voltammetry for measurement of electrode reaction kinetics, Anal. Chem., 37 (1965) 1351-1355.

[56] X. Niu, M. Lan, H. Zhao, C. Chen, Highly sensitive and selective nonenzymatic detection of glucose using three-dimensional porous nickel nanostructures, Anal. Chem., 85 (2013) 3561-3569.

[57] F. Anson, Application of potentiostatic current integration to the study of the adsorption of cobalt (III)-(ethylenedinitrilo (tetraacetate) on mercury electrodes, Anal. Chem., 36 (1964) 932-934.

[58] L. Wu, X. Zhang, J. Chen. A new third-generation biosensor for superoxide anion based on dendritic gold nanostructure, J. Electroanal. Chem., 2014, 726: 112-118.

[59] A. S. Jalilov, C. Zhang, E. L. Samuel, W. K. Sikkema, G. Wu, V. Berka, T. A. Kent, A. L. Tsai, J. M. Tour, Mechanistic study for the conversion of superoxide to oxygen and hydrogen peroxide in carbon nanoparticles, ACS Appl. Mater. Interfaces, 24 (2016) 15086-15092.

[60] E. L. Samuel, D. C. Marcano, V. Berka, B. R. Bitner, G. Wu, A. Potter, R. H. Fabian, R. G. Pautler, T. A. Kent, A. L. Tsai, Highly efficient conversion of superoxide to oxygen using hydrophilic carbon clusters, Proc. Natl. Acad. Sci., 112 (2015) 2343-2348.

[61] S. Osuna, M. Swart, M. Solà, On the mechanism of action of fullerene derivatives in superoxide dismutation, Chem. Eur. J., 16 (2010) 3207-3214.

[62] G. F. Liu, M. Filipović, I. Ivanović-Burmazović, F. Beuerle, P. Witte, A. Hirsch, High catalytic activity of dendritic C60 monoadducts in metal-free superoxide dismutation, Angew. Chem.-Int. Edit., 47 (2008) 3991-3994.

[63] F. Dashtestani, H. Ghourchian, K. Eskandari, H. A. Rafiee-Pour, A superoxide dismutase mimic nanocomposite for amperometric sensing of superoxide anions, Microchim. Acta, 182 (2015) 1045-1053.

[64] M. Wang, Y. Han, X. Liu, Z. Nie, C. Deng, M. Guo, S. Yao, Assembly of layer-by-layer films of superoxide dismutase and gold nanorods: A third generation biosensor for superoxide anion, Sci. China-Chem., 54 (2011) 1284-1291.

[65] T. Liu, X. Niu, L. Shi, X. Zhu, H. Zhao, M. Lana, Electrocatalytic analysis of superoxide anion radical using nitrogen-doped graphene supported Prussian Blue as a biomimetic superoxide dismutase, Electrochim. Acta, 176 (2015) 1280-1287.

[66] P. Santhosh, K. M. Manesh, S. H. Lee, S. Uthayakumar, A.I. Gopalan, K. P. Lee, Sensitive electrochemical detection of superoxide anion using gold nanoparticles distributed poly (methyl methacrylate)-polyaniline core-shell electrospun composite electrode, Analyst, 136 (2011) 1557-1561.

# Figure caption

**Fig. 1.** SEM and TEM (inset) images of SCS (A), HMCS (B) and N-HMCS (C). The nitrogen adsorption-desorption isotherms and pore size distribution curves (inset) of SCS (D), HMCS (E) and N-HMCS (F).
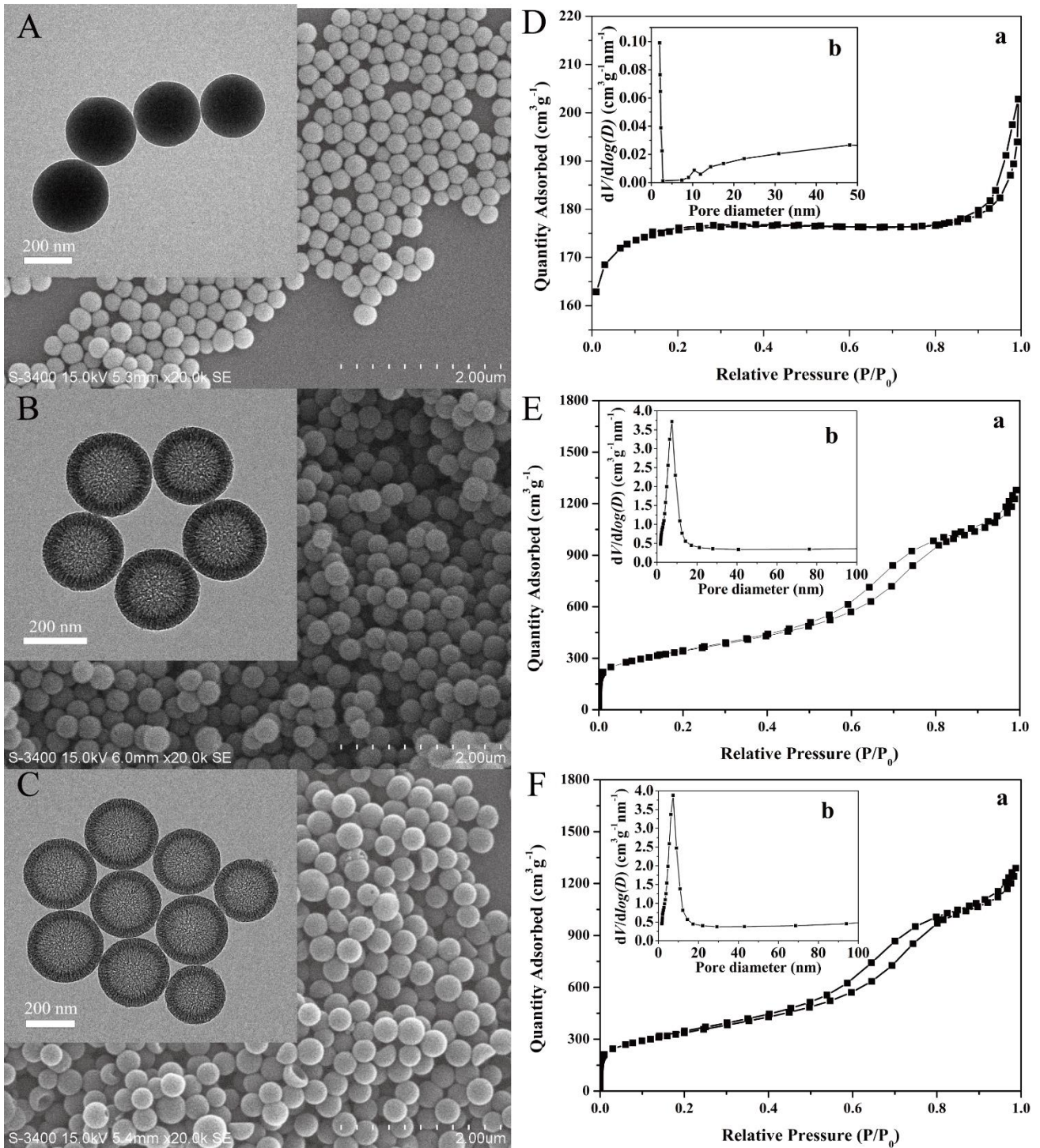
**Fig. 2.** (A) N1s spectrum of N-HMCS. (B) Raman spectra of SCS, HMCS and N-HMCS.
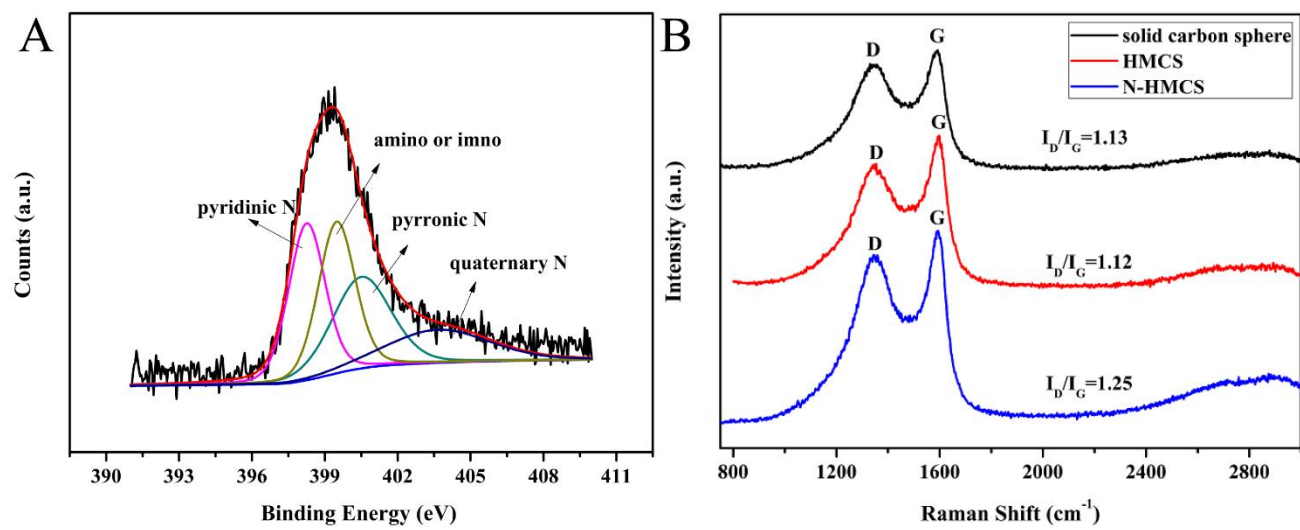
**Fig. 3.** (A) CV curves of SPCE, SCS/SPCE, HMCS/SPCE and N-HMCS/SPCE in 5 mM $K_3[Fe(CN)_6]$ at a scan rate of 20 mV s$^{-1}$. (B) Nyquist plots of SPCE, SCS/SPCE HMCS/SPCE and N-HMCS/SPCE in 5 mM $K_3Fe(CN)_6$ and 0.1 M KCl solution and inset is the equivalent circuit. (C) Chronocoulometric plots of the SPCE, SCS/SPCE, HMCS/SPCE and N-HMCS/SPCE in 0.1 mM $K_3[Fe(CN)_6]$ and 1 M KCl with the potential range from -0.1 to 0.3 V, and the sample interval as $1\times10^{-5}$ s; the inset shows relationship between Q and t$^{1/2}$. (D) CV curves of N-HMCS/SPCE in 0.1 M PBS (pH 7.4, containing 5 mM $K_3[Fe(CN)_6]$ and 0.1 M KCl) at different scan rates. The inset of (D) is the redox peak current as a function of the square root of scan rate.
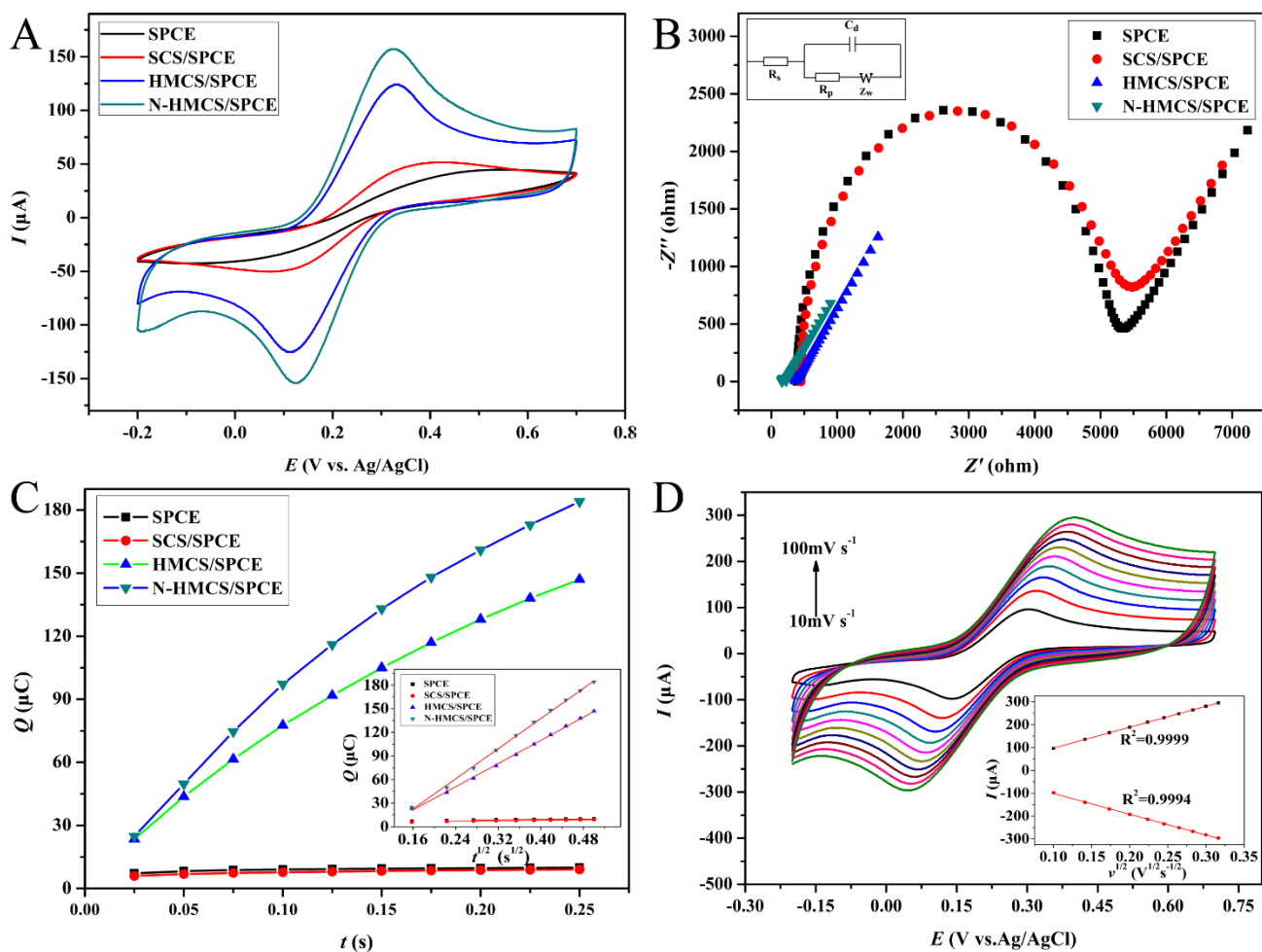
**Fig. 4.** CV curves of HMCS/SPCE (A) and N-HMCS/SPCE (B) in 0.1 M deoxidized PBS (pH 7.4) with the absence and presence of 400 μM $O_2^{\bullet-}$ at a scan rate of 50 mVs$^{-1}$. (C) Comparison of current-time response of SCS/SPCE, HMCS/SPCE and N-HMCS/SPCE for $O_2^{\bullet-}$ at -0.25, -0.25 and -0.15 V, respectively. (D) Current-time response of N-HMCS/SPCE with successive injection of $O_2^{\bullet-}$ into 0.1 M deoxidized PBS (pH 7.4) at -0.15 V.
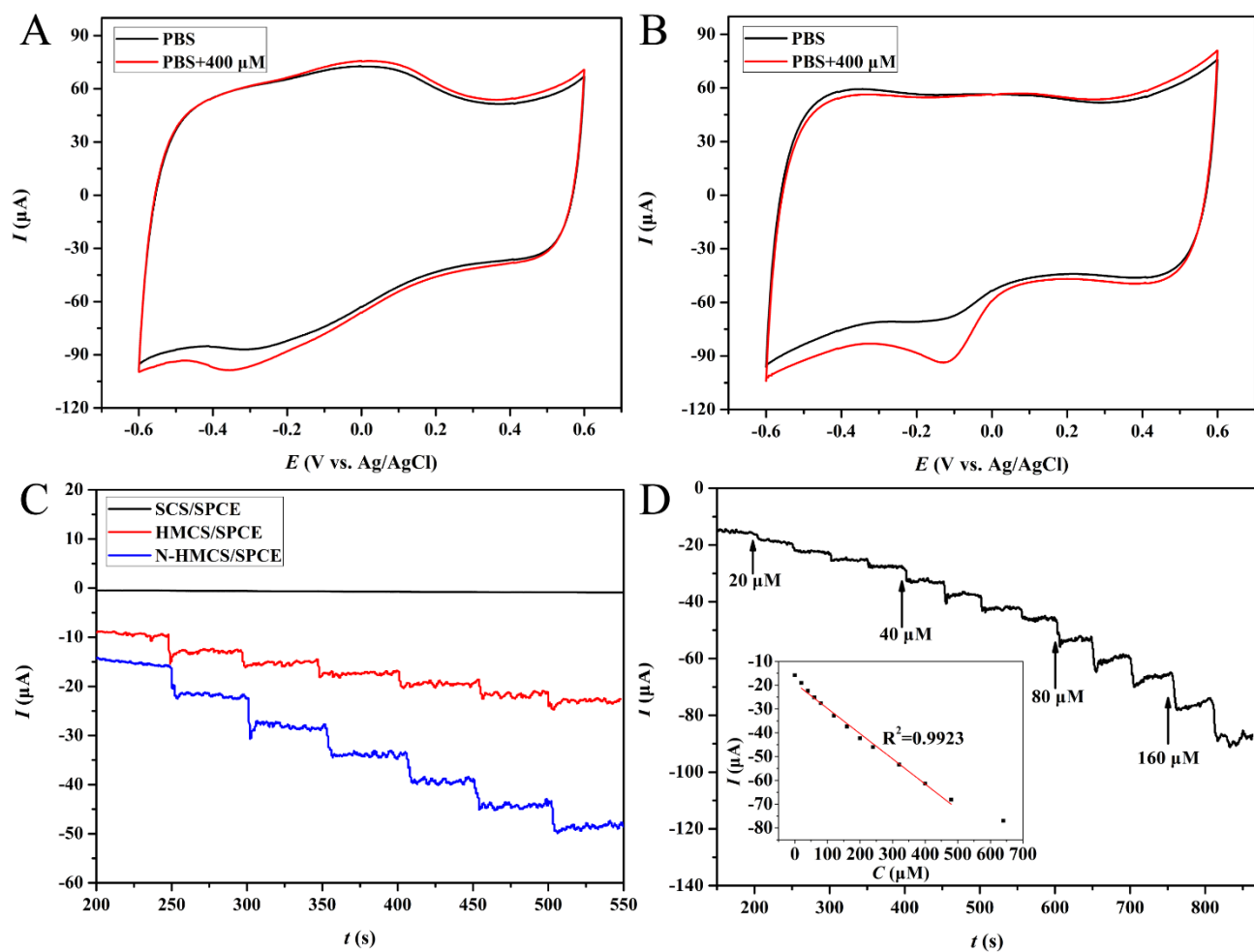
**Table 1.** Comparison of the analytical performance of various electrodes for $O_2^{\cdot-}$ detection

| Electrode | Application potential (V) | Sensitivity ($\mu A$ $cm^{-2}$ $mM^{-1}$) | Linear range ($\mu M$) | Limit of detection ($\mu M$) | Ref. |
|---|---|---|---|---|---|
| **N-HMCS/SPCE** | **-0.15** | **1493.2** | **20~480** | **2.2** | **This work** |
| GNPs/Cu-Cys | 0.25 | 18 | 3.1~326 | 2.8 | [63] |
| PDDA/MWCNTs－Pt/GCE | -0.5 | 863.41 | 0.7-3000 | 0.1 | [11] |
| (SOD/AuNRs)/Cys/Au | -0.15 | 22.11 | 0.2~200 | 0.1 | [64] |
| PB-NGS/SPCE | -0.05 | 318 | 0~1456 | 1.2 | [65] |
| PMMA/PANI-nanoAu/SOD-ESCFM | 0.3 | 42.5 | 0.5~2.4 | 0.3 | [66] |
| SOD/PtPd/MWCNTs/SPGE | -0.1 | 601 | 40~1550 | 0.71 | [47] |